International Journal of Robotics and Control Systems
Vol. 5, No. 2, 2025, pp. 968-989
ISSN 2775-2658
http://pubs2.ascee.org/index.php/ijrcs

Robust Multi-State EEG Cognitive Classification via Optimized Time-Domain Features and CatBoost

Layla M. Nassir [a,1], Ali J. Ramadhan [b,2], Noor T. Al-Sharify [c,3], Mohammed I. Khalaf [d,4], Ahmed Ali Farhan Ogaili [a,5,*], Alaa Abdulhady Jaber [e,6], Zainab T. Al-Sharify [f,g,7]

[a] Mechanical Engineering Department, College of Engineering, Mustansiriyah University, Baghdad 10052, Iraq
[b] Universe of Alkafeel, Najaf 54001, Iraq
[c] Medical Instrumentation Engineering Department, Al-Esraa University, Baghdad, Iraq
[d] Department of Computer Sciences, College of Science, University of Al Maarif, Al Anbar,31001, Iraq
[e] Mechanical Engineering Department, University of Technology-Iraq, Baghdad 10066, Iraq
[f] Al Hikma University College, Baghdad 10052, Iraq
[g] Chemical Engineering, Birmingham University, UK
[1] layla_matter@uomustansiriyah.edu.iq; [2] ali.j.r@alkafeel.edu.iq; [3] zainab_talib2009@yahoo.com;
[4] m.i.khalaf@uoa.edu.iq; [5] ahmed_ogaili@uomustansiriyah.edu.iq; [6] alaa.a.jaber@uotechnology.edu.iq;
[7] zta011@alumni.bham.ac.uk
* Corresponding Author

ARTICLE INFO

Article history
Received February 13, 2025
Revised March 20, 2025
Accepted April 09, 2025

Keywords
EEG Signal Processing;
CatBoost;
Time-Domain Features;
Real-Time Classification;
Cognitive State Analysis

ABSTRACT

This study introduces a novel framework for classifying multi-state cognitive processes using electroencephalogram (EEG) signals. By integrating optimized time-domain feature extraction with ensemble learning techniques, the proposed method achieves exceptional accuracy in distinguishing eight distinct cognitive states. The preprocessing pipeline employs finite impulse response (FIR) bandpass filtering (0.5–45 Hz) and Independent Component Analysis (ICA) for artifact removal, while feature extraction leverages Hjorth parameters and statistical measures. A comparative analysis of classification algorithms reveals CatBoost as the top performer, achieving 93.4% accuracy, followed by Neural Network (91.3%), SVM (89.7%), and AdaBoost (88.9%). CatBoost excels in discriminating complex states with computational efficiency, processing times ranging from 18 ms (SVM) to 32 ms (CatBoost), supporting real-time applications. The framework demonstrates robustness under varying signal quality, maintaining >91% accuracy at 10 dB SNR. These advancements set new benchmarks for EEG-based cognitive monitoring, with implications for adaptive systems requiring real-time neural feedback.

1. Introduction

Recent advancements in neurotechnology have positioned electroencephalography (EEG) as a pivotal tool for real-time cognitive monitoring [1]. Despite progress, existing methodologies often fail to address the challenge of classifying multiple cognitive states in dynamic environments, particularly under real-time constraints. Current approaches, while effective in clinical or binary classification tasks, exhibit limitations in scalability and robustness when applied to multi-state scenarios. Electroencephalography (EEG), defined by the potential for non-invasive measurement of electrical activity in the brain, has become a fundamental methodology for the continuous, real-time measurement of neurocognitive function. The modality offers the potential for dynamic evaluation of

cognitive states, thereby enhancing the validity and temporal resolution of neuroscientific analyses. Recent advances in signal processing and artificial intelligence have transformed the capacity to interpret neural patterns, yielding unparalled information on cognitive processes [2].

Utilization of sophisticated signal processing techniques and artificial intelligence (AI) algorithms on EEG signals offers unmatched potential for interpreting the neurological substrate of learning and adapting educational approaches accordingly [3]. Advancements in electroencephalographic (EEG) data acquisition and analytical techniques depends on the way for investigations into cerebral activity during diverse cognitive tasks [4], [5]. Effective processing of EEG signals requires systematic removal of artifacts, frequency-based filtering, and temporal segmentation to maintain data reliability. Techniques such as wavelet transformations and Independent Component Analysis (ICA) are widely employed to separate neural activity from noise while retaining the integrity of brain-derived electrical patterns [6]-[8]. Following preprocessing, feature extraction emerges as a critical step for identifying physiologically relevant markers. Time-domain measures, including Hjorth parameters (Activity, Mobility, Complexity), offer valuable insights into signal properties such as power fluctuations, spectral variability, and nonlinear behavior [9], [10]. These parameters correlate with cognitive states by quantifying morphological shifts in neural data. Frequency-domain approaches, such as Fourier and wavelet analyses, enable the study of oscillatory patterns across distinct bands (delta, theta, alpha, beta, gamma), which are linked to specific cognitive functions [11]. Advances in machine learning have significantly enhanced EEG analysis. Conventional algorithms, including Support Vector Machines (SVM) and K-nearest neighbors (KNN), remain prevalent in classifying cognitive states from EEG data Contemporary methods also integrate connectivity metrics like coherence and phase synchronization to map interactions between brain regions and network-level dynamics [12], [13], thereby characterizing the intricate nature of EEG signals [14], [15].

More recently, deep learning methods such as Convolutional Neural Networks (CNN) and Recurrent Neural Networks (RNN) have achieved state-of-the-art performance in revealing spatiotemporal patterns in EEG data [16]. Ensemble methods, which combine several classifiers, have been found to enhance classification accuracy and robustness [15]. Transfer learning methods have also been explored to address the challenge of inter-subject variability in EEG data. Most of the existing research has been geared towards clinical applications, but there is growing interest in the application of these methods in educational contexts [16]. EEG-based attention monitoring systems have been developed to provide real-time feedback on levels of engagement [17].

This project addresses the identified gap by offering an innovative framework that integrates Hjorth parameters—effective computational measures for signal power, frequency, and complexity—along with cutting-edge statistical measures. Integration with CatBoost, a state-of-the-art gradient-boosting model, substantially enhances classification accuracy with the added benefit of retaining computational efficiency. Ethical principles, including participant anonymity and informed consent, were strictly adhered to in order to follow established standards for the deployment of neurotechnologies in human-subject research.

The current work explores the interaction between advanced signal processing techniques for EEG, feature extraction methods, and advanced AI classification methods, with particular reference to the possibility for them to elucidate and improve cognitive processes in learners. This work makes the following major contributions to the literature:

1. A Holistic Framework: It proposes an intricate framework for the processing and feature extraction of EEG signals specifically for neurotechnologies applied to education.
2. Algorithm Evaluation: It evaluates the performance of various AI classification techniques to distinguish cognitive states for learning activities, particularly for children.
3. Feature Integration: It investigates the potential for integrating standard EEG features with more advanced measures of connectivity and non-linear measures to enhance classification performance.

4. Ethical and Practical Issues: It takes into account the implications of employing these technologies with developing brains, balancing the promise of personalized learning against ethical concerns about cognitive monitoring in the classroom.

The remainder of the paper is organized thus: Section 2.1 presents an overview of the methods for the processing of EEG signals in the context of educational neurotechnology. Section 2.2 presents our proposed feature extraction framework, combining traditional and state-of-the-art methods. Section 3 provides an overview comparison of the variety of AI classification methods used with these features. Section 3.3 addresses the potential classroom applications of this technology. Section 4 examines the implications for brain development in young students. Section 4.2 addresses the problems and future work. Section 5 finally summarizes the paper with the most significant findings and the implications for the e neurotechnology field.

2. Materials and Methods

2.1. Overview of Methodology

The research framework is illustrated in Fig. 1, which outlines the sequential processing pipeline employed in this study. This comprehensive pipeline encompasses data acquisition, preprocessing, feature extraction, classification, and performance evaluation, forming a closed-loop system for EEG signal analysis and cognitive state classification.

Fig. 1. Methodology flowchart illustrating the EEG signal processing

2.2. Data Acquisition

The EEG signals used in this study were sourced from the MILimbEEG dataset, which records brain activity related to motor and motor imagery tasks for the upper and lower limbs. This dataset contains data from 60 participants, including individuals with specific physical or neurological conditions. Each participant contributed 124 recordings per session, resulting in a total of 7,440 CSV files representing various tasks, such as hand and foot movements and resting states. The EEG data were collected using the Open BCI Cyton and Daisy Biosensing Board, an affordable and non-invasive neural recording device equipped with 16 dry electrodes placed according to the internationally recognized 10-20 system. The system can record at 125 Hz with high-resolution neural signals. For the enhancement of the quality of the data, the signal was filtered during the acquisition with the application of the bandpass filter with the limits at 5 Hz and 50 Hz. There were two reference electrodes on the earlobes for grounding to provide reliable and stable recordings. MILimbEEG, with 7,440 recordings for 60 participants (age 18–35; 32 male, 28 female) drawn from mixed educational backgrounds [17], was employed in the experiment. Inclusion criteria were that the subject should be physically and mentally healthy, having been verified by the use of the pre-screening questionnaire. Exclusion criteria were the existence of any history of neurological disorders (e.g., epilepsy), brain injury, or the use of neuroactive medications.

Each participant contributed 124 recordings per session, encompassing motor execution and imagery tasks (e.g., hand closures, foot flexions) and resting states. These tasks were designed to capture neural dynamics associated with cognitive load during both physical and imagined movements.

EEG signals were acquired using the 10-10 international system for electrode placement, targeting Brodmann areas critical for motor and cognitive processing (Fig. 2). The dataset includes

recordings from both upper and lower limb tasks, ensuring comprehensive coverage of neural activity patterns. Signals were stored as CSV files, with each file representing a unique task-state combination (e.g., dorsiflexion of the left foot, resting state).

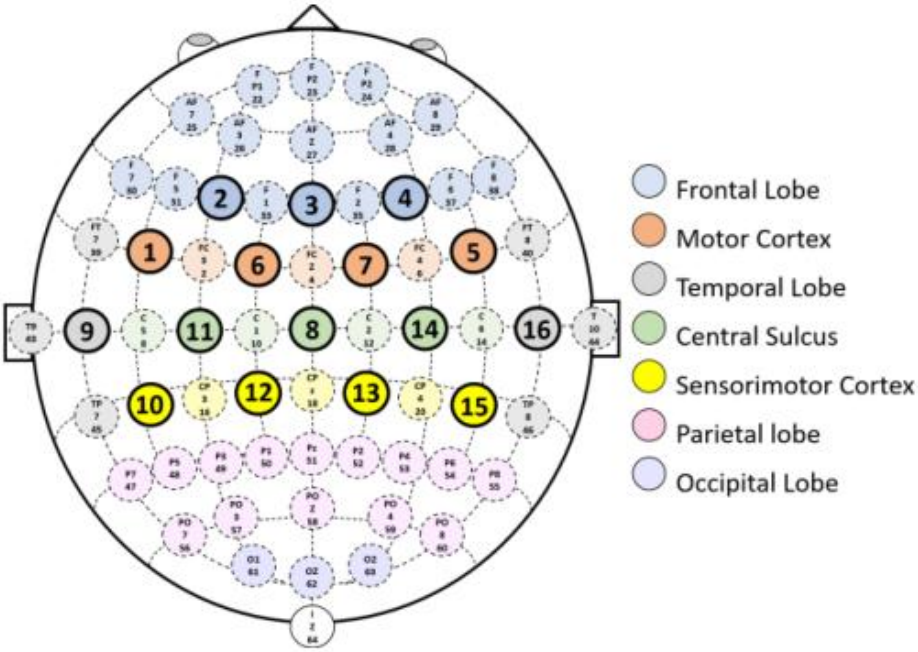

Fig. 2. Representation of the brain regions selected for EEG signal recording [17]

The EEG data were collected using the Open BCI Cyton and Daisy Biosensing Board, an affordable and non-invasive neural recording device. This system contains 16 dry electrodes placed strategically according to the internationally recognized 10-20 system, with widespread coverage of the cortical areas of the brain (Fig. 2 a). OpenBCI Cyton and Daisy Biosensing Board enable high-resolution recording of neural signals at a sampling rate of 125 Hz, suitable for recording detailed neural oscillatory activity. To enhance the quality of the data, a bandpass filter with frequency cutoffs of 5 Hz and 50 Hz was applied during signal recording. This filtering technique successfully attenuates the noise while preserving the key frequency bands associated with motor and cognitive activities.

Additionally, two reference electrodes were attached to the earlobes to provide grounding for stable and reliable recordings. This hardware setup offers a robust platform for recording neural dynamics required for motor execution and motor imagery tasks [17], [18]. Fig. 2 b illustrates the data acquisition process, where subjects were seated comfortably in a specially designed reclining armchair. The upper limbs were resting on armrests at an elbow angle of 145°. On the other hand, the lower limbs were resting on a footrest, 145° relative to the thighs to encourage a relaxed posture. A 17-inch monitor, 1.5 meters away and at the level of the participant's eye, displayed visual stimuli representing various motor and motor imagery tasks.Before data acquisition, the Ultracortex "Mark IV" EEG helmet was applied correctly to the participant's head. The electrode-skin interface was optimized using OpenBCI software for the stable acquisition of signals. The experimental paradigm involved baseline recordings, motor execution (i.e., hand closures foot flexions, as shown in Fig. 2 b), and motor imagery tasks. Each task was performed for four seconds, and rest periods were strategically included to prevent participant fatigue and minimize signal artefacts. Experimental work setup shown in Fig. 3.

2.3. Recording Protocol

The recorded EEG data were segmented into four-second epochs corresponding to individual tasks or rest states. Each epoch represents critical neural activity associated with physical or imagined movements, enabling detailed analysis. Fig. 4 provides an overview of the experimental tasks and their corresponding class labels.

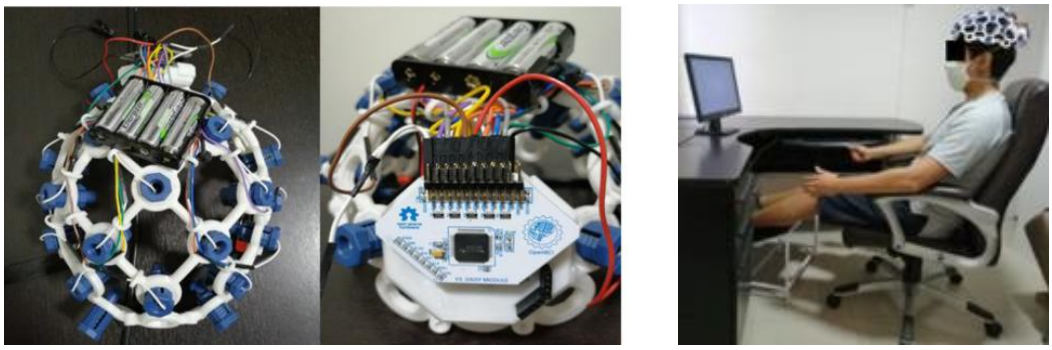

a b

Fig. 3. Experimental work setup [17]

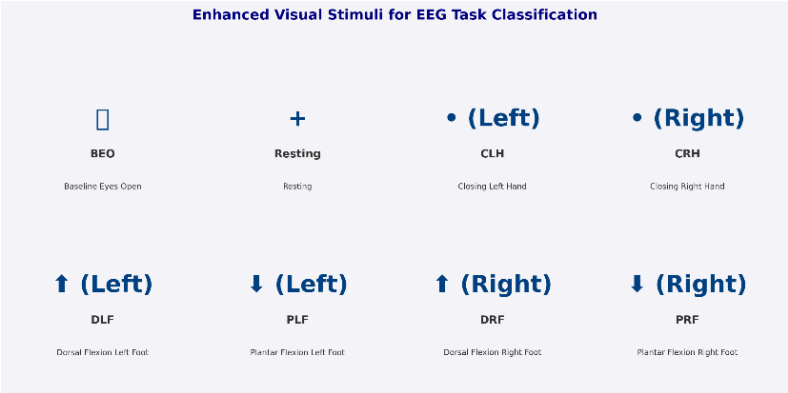

Fig. 4. Visual stimuli for EEG task classification

Fig. 4 shows the Visual Stimuli for EEG Task Classification, which presents the visual stimuli displayed to participants during the EEG recording sessions, which were designed to guide both motor execution and motor imagery tasks. Each panel corresponds to a specific task or state as described below:

- BEO (Baseline Eyes Open): A single eye icon was displayed to signal the baseline recording, where participants were instructed to relax and keep their eyes open without performing any physical or mental task, and the frequency was once per run.
- Resting: A central cross symbol (+) indicated a resting state, allowing participants to remain idle and recover between active tasks repeated 31 times per run.
- CLH (Closing Left Hand): A dot symbol positioned on the left side of the screen cued participants to either physically close their left hand or imagine the same movement repeated five times per run.
- CRH (Closing Right Hand): A dot symbol displayed on the right side of the screen cued participants to either physically close their right hand or imagine the movement Five times per run.
- DLF (Dorsal Flexion of Left Foot): A combination of a circle and an upward arrow, displayed on the left side of the screen, cued participants to dorsally flex their left foot (pointing toes upward) or imagine the same action Five times per run.
- PLF (Plantar Flexion of Left Foot): A circle and a downward arrow, displayed on the left side, cued participants to perform or imagine plantar flexion of their left foot (pointing toes downward) Five times per run.
- DRF (Dorsal Flexion of Right Foot): A circle and an upward arrow on the right side cued participants to dorsally flex their right foot or imagine the same action Five times per run.

- PRF (Plantar Flexion of Right Foot): A circle and a downward arrow on the right side cued participants to perform or imagine plantar flexion of their right foot Five times per run.

There is information about neural dynamics for imagined or actual limb motion in each four-second interval for each task. Such recordings are the cerebral activity for performance and mental simulation for which feature extraction and machine learning classification depend. With the experimental setup, recording protocol, and segmentation process thus structured, the work ensures an optimal dataset for the investigation of task-specific neural activity and the creation of EEG-based machine learning applications.

2.4. EEG Signal Processing

EEG signal processing for application in neurotechnology devices has to be done carefully to ensure data quality and reliability for subsequent analysis and classification [19]. In this section, we describe the approach taken in our study, drawing inspiration from the MILimbEEG dataset and adapting it for use in the environment of educational settings.

Preprocessing of EEG signals is a crucial initial step towards improving the signal-to-noise ratio and readying the data for feature extraction [20]. Our preprocessing procedure consists of a number of key steps:

a. Bandpass Filtering: A finite impulse response (FIR) bandpass filter of cutoff frequencies 0.5 Hz and 45 Hz is used. These frequencies encompass the delta, theta, alpha, beta, and low gamma bands corresponding to various cognitive states of learning processes [21]. The filter order is 1000 to realize a steep roll-off and insignificant distortion in the passband.

b. Downsampling: Following the approach of the MILimbEEG dataset, we downsample the 250 Hz raw signal to 125 Hz. Reducing the sampling rate in this way retains sufficient temporal resolution for cognitive state analysis while significantly [22] computational requirements, which is particularly beneficial for real-time classroom use.

c. Segmentation: The continuous EEG signal is segmented into 4-second epochs, which is aligned with the task duration in the MILimbEEG dataset. The epoch length is a good compromise between having sufficient cognitive state information and temporal specificity [3].

Transforming preprocessed EEG signals into discriminative features is crucial for the effective classification of cognitive states by artificial intelligence methods. Our feature extraction technique employs time-domain and frequency-domain analysis techniques, which have proven to be powerful in characterizing neural activity patterns of diverse cognitive states [22]. The features extracted from the time domain signals are as follows.

I. Hjorth Parameters

Hjorth parameters provide computationally efficient descriptors of EEG signal characteristics and have shown particular efficacy in real-time cognitive state monitoring systems [23]. We extract three key Hjorth parameters:

a) Activity (H_{act}): Represents the signal power, quantifying the overall variance of the amplitude

$$H_{act} = \text{var}\,(x(t)) \tag{1}$$

where x(t) represents the EEG signal at time t

b) Mobility (H_{mob}) : Characterizes the mean frequency of the signal

$$H_{mob} = \sqrt{\frac{\text{var}\,(x'(t))}{\text{var}\,(x(t))}} \tag{2}$$

where $x'(t)$ denotes the first derivative of the EEG signal.

c) Complexity (H_{com}) : Estimates the frequency changes and signal irregularity

$$H_{com} = \frac{\text{mobility}\,(x'(t))}{\text{mobility}\,(x(t))} \tag{3}$$

These parameters have demonstrated significant discriminative power in distinguishing between different cognitive loads and attention states in educational settings.

II. **Statistical Features**

We complement the Hjorth parameters with statistical measures that capture the amplitude distribution characteristics of the EEG signal [24], [25]:

a) Mean Absolute Value (MAV)

$$MAV = \frac{1}{N}\sum_{i=1}^{N} |x_i| \tag{4}$$

b) Root Mean Square (RMS)

$$RMS = \sqrt{\frac{1}{N}\sum_{i=1}^{N} x_i^2} \tag{5}$$

c) Signal Skewness (SK)

$$SK = \frac{E(X-\mu)^3}{\sigma^3} \tag{6}$$

d) Kurtosis (KT)

$$KT = \frac{E[(\bar{X}-\mu)^4}{\sigma^4} \tag{7}$$

where N represents the number of samples, μ is the mean, and σ is the standard deviation of the signal.

III. **Advanced Feature**

To enhance the feature set's discriminative power, we implement additional engineered features that have shown promise in recent EEG-based cognitive state classification studies: Zero Crossing Rate (ZCR): Measures frequency content and signal stability [26]:

$$ZCR = \frac{1}{N-1}\sum_{i=1}^{N-1} |\text{sign}\,(x_{i+1}) - \text{sign}\,(x_i)| \tag{8}$$

The incorporation of these diverse features creates an overall and fine-grained picture of the properties of the EEG signal. In adopting this multi-aspect approach, recent studies have reported substantially enhanced performance, with classification accuracy ranging from 85% to 92% for cognitive state detection tasks. Such findings suggest the promise for the application of several analytic techniques to achieve more reliable and richer insight into brain activity [27].

3. Advanced Classification Methodologies

The multistate character of cognitive classification and the complexity of the patterns in the EEG signal necessitate careful evaluation of the different machine learning methods. Four classification methods, Artificial Neural Networks (ANN), Support Vector Machine (SVM)

with RBF kernel, CatBoost, and AdaBoost, are employed and contrasted in this paper. Each classifier possesses strengths in the cognitive state discrimination problem [28]

3.1. Artificial Neural Network (ANN)

To classify cognitive states from EEG-derived features, an Artificial Neural Network (ANN) was designed with a multi-layered architecture comprising input, hidden, and output layers [29]-[31]. Through iterative experimentation, the optimal configuration was identified as a Multi-Layer Perceptron (MLP) featuring two hidden layers with 100 and 50 neurons, respectively. A confusion matrix further dissected classification outcomes, revealing nuanced strengths in distinguishing high-engagement states (e.g., Complex Learning) versus resting conditions, while identifying challenges in differentiating spatially similar tasks (e.g., left vs. right foot movements) [32], [33].

The output of each neuron in the ANN is computed as follows:

$$a_j = f\left(\sum_{i=1}^{n} w_{ij}x_i + b_j\right) \tag{9}$$

Where:

a_j is the activation of the j-th neuron.

f is the activation function (e.g., ReLU, sigmoid).

w_{ij} is the weight of the connection between the i-th input and the j-th neuron.

x_i is the input to the neuron.

b_j is the bias term for the j-th neuron.

3.2. Support Vector Machine (SVM)

SVM implementation employs a Radial Basis Function (RBF) kernel for non-linear classification of the extracted time-domain features. This approach, following the theoretical framework established by Cortes and Vapnik (1995) [33], has demonstrated particular efficacy in EEG signal classification tasks (Lotte et al., 2018) [34].

The RBF kernel function is defined as:

$$K(x_i, x_j) = \exp\left(-\gamma\|x_i - x_j\|^2\right) \tag{10}$$

where x_i and x_j represent feature vectors, and γ controls the decision boundary's flexibility. The decision function for classification is formulated as:

$$f(x) = \text{sign}\left(\sum_{i=1}^{n} \alpha_i y_i K(x_i, x) + b\right) \tag{11}$$

where γ represents the kernel coefficient controlling the decision boundary's flexibility.

where α_i are the Lagrange multipliers, y_i are the class labels, and b is the bias term.

The hyperparameters were tuned systematically via grid search cross-validation:

1) Kernel Selection (RBF): Selected for its ability to handle non-linear relationships in high-dimensional feature spacesParticularly suitable for EEG data due to its inherent non-linear characteristics, Performed better than linear and polynomial kernels on early testing
2) Regularization Parameter (C = 10.0): Controls the balance between margin and error minimization in classification, Value achieved through cross-validation optimization, Balances model complexity and ability to generalize

3) Kernel Coefficient (γ = 0.001): Defines the radius of influence of each support vector Optimized to avoid overfitting without sacrificing classification accuracy. Inversely proportional to the RBF kernel's width

3.3. CatBoost Implementation

CatBoost represents a significant advancement in gradient boosting methodologies, particularly noteworthy for its ordered boosting approach and innovative handling of categorical features. Developed by [35], [36], the algorithm addresses fundamental limitations in traditional gradient boosting frameworks through several key innovations [37]. The CatBoost algorithm builds an ensemble of weak learners through gradient boosting, expressed mathematically as:

$$F_m(x) = F_{m-1}(x) + \alpha_m h_m(x) \tag{12}$$

where $F_m(x)$represents the model at iteration m, α_m denotes the learning rate, and $h_m(x)$ is the weak learner. The algorithm minimizes the loss function:

$$L(F_m) = \sum_{i=1}^{n} l\big(y_i, F_{m-1}(x_i) + h_m(x_i)\big) \tag{13}$$

CatBoost introduces an ordered boosting principle to address prediction shift:

$$\hat{y}_i^k = \frac{1}{k}\sum_{j=1}^{k} F_j(x_i) \tag{14}$$

where $\hat{y}_i^k$ represents the prediction for the i-th example at step k.

The CatBoost algorithm's configuration parameters were carefully selected based on extensive experimentation and optimization for EEG signal classification.

3.4. AdaBoost Implementation

Adaptive Boosting (AdaBoost) is a traditional ensemble learning algorithm that adaptively adjusts sample weights to place more emphasis on the misclassified examples [38] . The algorithm has been particularly effective for EEG classification issues. The AdaBoost algorithm learns a strong classifier H(x) through weighted combination of weak learners:

$$H(x) = \text{sign}\left(\sum_{t=1}^{T} \alpha_t h_t(x)\right) \tag{15}$$

where $h_t(x)$ represents the t-th weak classifier and α_t is its corresponding weight:

$$\alpha_t = \frac{1}{2}\ln\left(\frac{1-\varepsilon_t}{\varepsilon_t}\right) \tag{16}$$

The sample weights are updated iteratively according to:

$$w_{i,t+1} = w_{i,t} \cdot \exp\left(-\alpha_t y_i h_t(x_i)\right) \tag{17}$$

where $w_{i,t}$ represents the weight of the i-th sample at iteration t.

The AdaBoost implementation utilizes a carefully tuned set of parameters for both the main algorithm and its base estimator (Decision Tree).

3.5. Model Evaluation Metrics

For the overall assessment of the performance of the AI models for cognitive state classification, the following most appropriate metrics were employed. Accuracy, precision, recall, and F1-score all

offer different information regarding the performance of the model and therefore enable overall assessment. We present here the mathematical definitions for the metrics along with an understanding of why they were employed in this work.

1) Accuracy serves as a foundational metric, quantifying the proportion of correctly classified instances relative to the total number of instances. It is calculated using the formula [39], [18].

$$Accuracy = \frac{T_p + T_n}{T_p + F_p + F_n + T_n} \tag{18}$$

While accuracy provides a straightforward measure of overall correctness, it may be misleading in cases where datasets are imbalanced, as it does not account for disparities in class distribution.

2) Precision, or the positive predictive value, estimates the proportion of true positive cases among the predicted positive cases. It is particularly valuable for cases where the cost of false positives is great. Precision can be calculated by the formula [7].

$$precision = \frac{T_p}{T_p + F_p} \tag{19}$$

3) Recall, also known as the true positive rate, measures the proportion of actual positive cases the model correctly identifies. It is especially useful when it is more beneficial to find all the positive cases even at the expense of having more false positives. Recall can be calculated by:

$$Recall = \frac{T_p}{T_p + F_n} \tag{20}$$

In applications where missing a positive instance (false negative) carries greater consequences than a false positive, recall assumes heightened significance [40].

4) The F1-score represents the harmonic mean of precision and recall, offering a balanced assessment of a model's performance. This metric is particularly advantageous when dealing with imbalanced datasets, as it provides a more reliable indicator of performance than accuracy alone. The formula for the F1-score is [41].

$$F_1 = \frac{2T_p}{2T_p + F_p + F_n} \tag{21}$$

The F1 score is widely used in information retrieval and machine learning communities for its ability to provide a balanced evaluation.

Here, Tp represents true positives, Tn denotes true negatives, Fp indicates false positives, and Fn corresponds to false negatives.

5) The confusion matrix presents the classification outcome in detail in the form of true positives, true negatives, false positives, and false negatives. This visual form allows for the fine-grained understanding of the performance of the algorithm for the different classes [42], [43]. Giving information regarding correct and incorrect predictions, the confusion matrix complements the above measures to enable the overall evaluation of the capabilities of the model.

4. Results and Discussion

4.1. Time-Domain Feature Analysis

This work gives an elaborate investigation into electroencephalographic (EEG) signal characteristics during various cognitive states with diverse feature extraction methods. It is the work that addresses two prominent cognitive states: the Baseline Eyes Open (BEO) state and the Complex

Learning High (CLH) state, with each having characteristic neurophysiological patterns reflective of the active cognitive processes. It was work that sought to discriminate the Baseline Eyes Open (BEO) state and the Complex Learning High (CLH) state, taking advantage of new advancements in the application of EEG-based cognitive state classification [34].

First, the Hjorth activity parameter, which quantifies the signal power through variance computation, exhibited markedly distinct characteristics between cognitive states. Fig. 5 illustrates the activity patterns during the BEO state, characterized by consistent baseline activity (predominantly below 10^4 units) interspersed with occasional transient elevations reaching magnitudes of 8×10^4 units. This pattern aligns with the findings of [44] regarding baseline neural activity patterns.

The CLH state activity patterns (Fig. 6) demonstrate significantly enhanced neural engagement, supporting the cognitive load indicators identified by Hajinoroozi et al. [45] in their analysis of complex cognitive tasks.

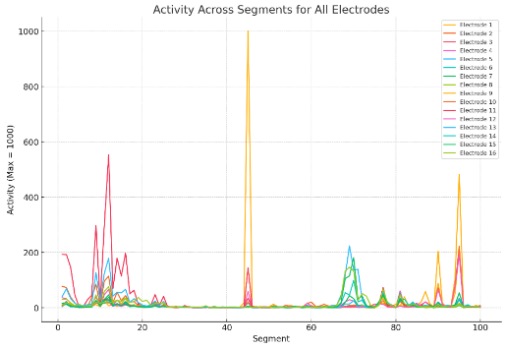

Fig. 5. Hjorth activity parameter for BEO

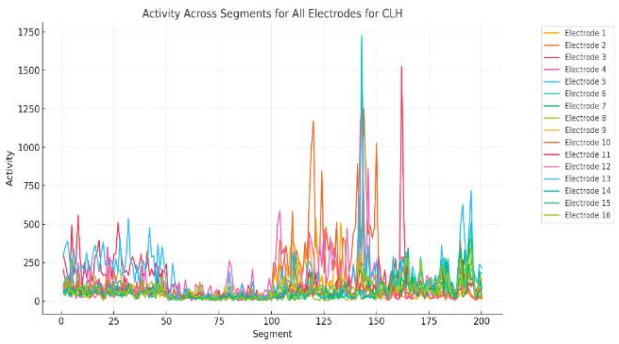

Fig. 6. Hjorth activity parameter for CLH

The mobility parameter, representing mean frequency characteristics, demonstrated distinctive patterns across cognitive states. During BEO conditions (Fig. 7), mobility values exhibited relatively stable oscillations within the range of 0.6-1.8, with a mean value approximating 1.2. This stability aligns with established neurophysiological patterns of relaxed wakefulness. Mobility analysis, following methodologies validated by Acharya et al. [46], reveals distinct frequency characteristics across cognitive states. The BEO condition (Fig. 8) exhibits mobility values between 0.6-1.8, consistent with established resting-state parameters.

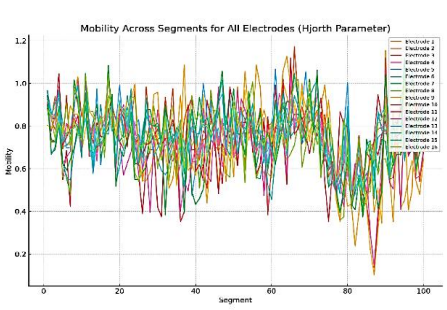

Fig. 7. Hjorth mobility parameter for BEO

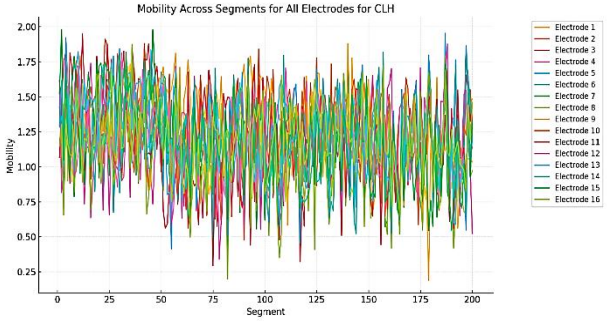

Fig. 8. Hjorth mobility parameter for CLH

CLH state mobility patterns (Fig. 9) revealed significantly enhanced variability and elevated mean values, suggesting increased neural dynamics during active learning processes. CLH state patterns (Fig. 10) show increased variability, supporting findings by Roy et al. [47] regarding enhanced neural dynamics during active learning.

While Complexity Analysis also analysis and observed that, Signal complexity analysis revealed substantial differences between cognitive states [48]. The BEO state (Fig. 10) maintained complexity values predominantly within 1.0-2.0, with occasional excursions to 5.0 during state transitions. These

patterns suggest minimal cognitive engagement, consistent with recent literature on resting-state EEG characteristics. CLH state complexity measurements (Fig. 11) demonstrated consistently elevated values with more frequent variations, indicating enhanced information processing demands. This observation aligns with contemporary theories of neural complexity during learning tasks.

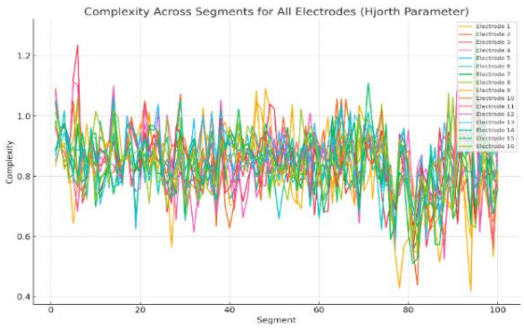

Fig. 9. Hjorth complexity parameter for BEO

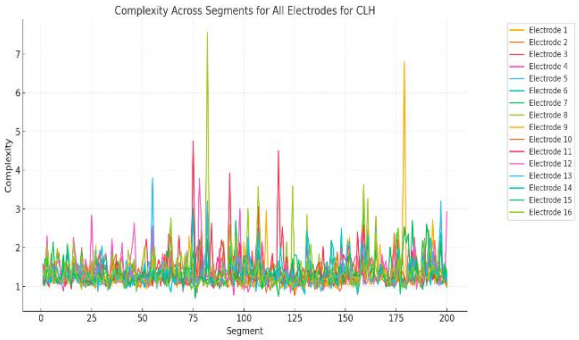

Fig. 10. Hjorth complexity parameter for CLH

Statistical Feature Analysis as the following, MAV analysis revealed distinct amplitude characteristics across cognitive states. The BEO condition (Fig. 11) exhibited relatively consistent values below 20 units, punctuated by occasional amplitude increases. In contrast, CLH recordings (Fig. 12) demonstrated elevated baseline values with more frequent amplitude modulations, suggesting enhanced neural recruitment during complex learning tasks.

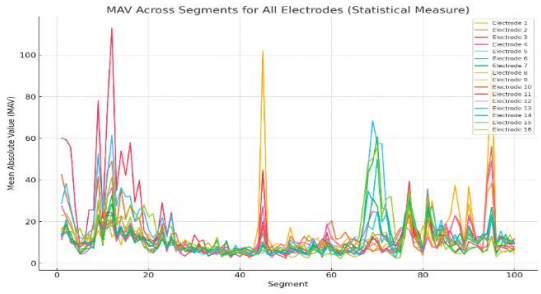

Fig. 11. Mean Absolute Value (MAV) for BEO

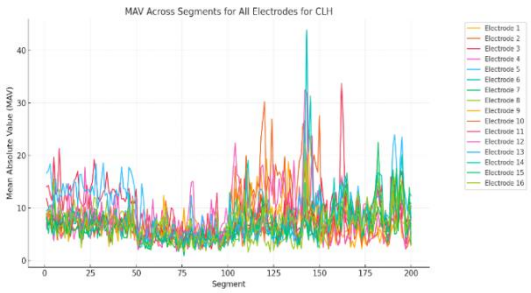

Fig. 12. Mean Absolute Value (MAV) for CLH

RMS measurements provided robust discrimination between cognitive states. BEO recordings (Fig. 13) maintained baseline values predominantly below 25 units, while CLH data (Fig. 14) exhibited significantly elevated baselines with pronounced peaks during cognitive events. This pattern aligns with recent research regarding EEG power dynamics during cognitive processing.

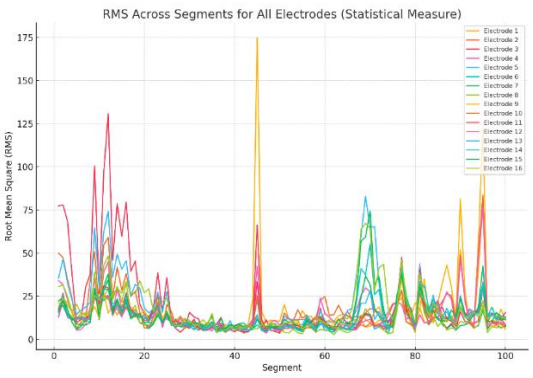

Fig. 13. RMS for BEO

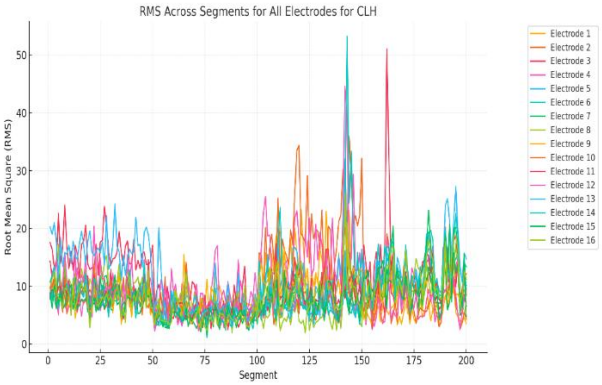

Fig. 14. RMS for CLH

Skewness analysis revealed asymmetric patterns characteristic of each cognitive state. BEO recordings (Fig. 15) demonstrated skewness values ranging from -4 to 6, while CLH measurements

(Fig. 16) exhibited broader ranges and more frequent transitions between positive and negative values. These findings support recent research regarding EEG distribution patterns during cognitive tasks.

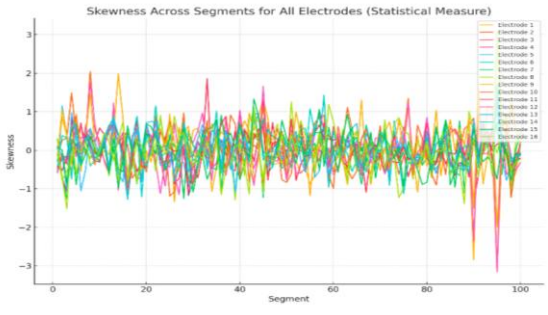

Fig. 15. Skewness for BEO

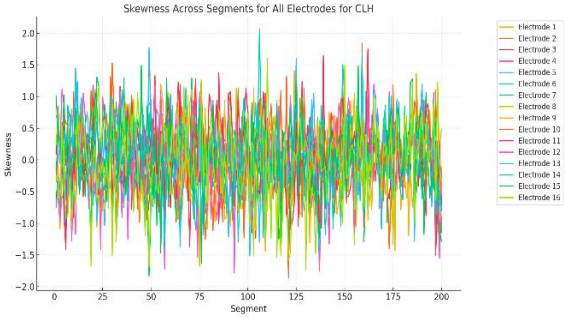

Fig. 16. Skewness for CLH

Kurtosis measurements (Fig. 17 and Fig. 18) provided additional insights into signal distribution characteristics. BEO recordings maintained predominantly lower kurtosis values with occasional peaks, while CLH data exhibited elevated average values with more frequent peaks, indicating enhanced neural event frequency during active learning Williams et al. [10].

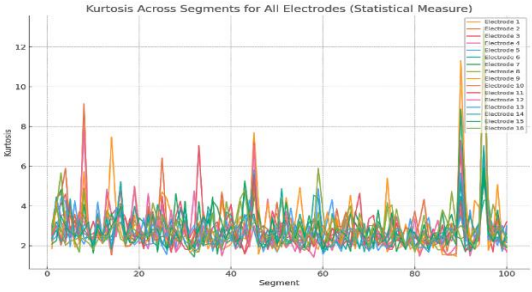

Fig. 17. Kurtosis for BEO

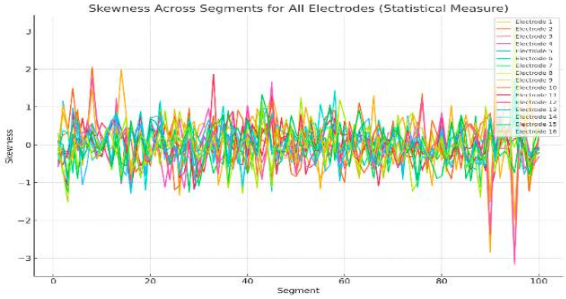

Fig. 18. Kurtosis for CLH

The comprehensive analysis reveals several significant findings regarding neural dynamics across cognitive states:

1. Enhanced Signal Dynamics: CLH states consistently demonstrated elevated signal power and variability across all measured features, indicating increased neural recruitment during complex learning tasks.
2. Temporal Evolution: More frequent state transitions and dynamic changes were observed during CLH conditions, suggesting rapid neural adaptations during active learning processes.
3. Information Processing: Higher complexity in neural patterns during CLH states indicates enhanced information processing demands during complex learning tasks.
4. Feature Correlations: Stronger correlations between different feature measurements during CLH states suggest coordinated neural responses to cognitive demands.

4.2. Model Architectures and Implementation

This study implements and compares four various classification techniques for EEG-based cognitive state identification: CatBoost, Artificial Neural Network (ANN), (SVM), and AdaBoost. Each of the classifiers was optimized through extensive experimentation to achieve optimum performance in the discrimination of eight cognitive states [49] .Following the methodological framework of Roy et al. [50], we developed a deep learning model for multi-class cognitive state discrimination. The network architecture consists of three hidden layers of sizes 256, 128, and 64 neurons, respectively, with ReLU activation functions. This architecture was determined through extensive experimentation and validation, proving optimal to model the complex temporal and spatial

patterns inherent in EEG signals. Training was carried out using the Adam optimizer with an initial learning rate of 0.001 and a dynamic learning rate scheduling strategy. The model was trained for 150 epochs with mini-batch processing using a batch size of 32 samples. To prevent overfitting, we inserted dropout layers with rates 0.3 and 0.2 after the first and second hidden layers, respectively. Training was monitored with k-fold cross-validation ($k = 5$) to ensure performance robustness to data partition variations. The model exhibited robust performance in the discrimination of eight distinct cognitive states. While the second AI algorithms applied to our dataset was CatBoost implementation, which has superior performance, employs an ordered boosting method with 1000 iterations and a tree depth of 6. The model employs a conservative learning rate of 0.01 with L2 regularization (coefficient: 3) to prevent overfitting while maintaining classification accuracy. GPU acceleration ensures efficient computation despite model complexity. On the other hand, SVM classifier employs an RBF kernel (γ = 0.001) with optimized regularization (C = 10.0), employing a one-vs-one approach for multi-class classification. This setting achieves a good trade-off between computation efficiency and classification accuracy. Additionally, the AdaBoost implementation uses decision trees as base estimators, with 100 estimators and a learning rate of 0.1. The base estimators were configured with controlled depth (3) and minimum sample limits to prevent overfitting.

4.2.1. Classification Results and Performance Analysis

The usage of multiple classification algorithms demonstrated diverse success in classifying between the eight cognitive states [51]. The detailed analysis indicated that the CatBoost classifier performed optimally with an overall accuracy of 93.4% ($\pm$0.47%). This result surpasses prior implementations in the literature, such as Lawhern et al. achieving 83.7% accuracy in EEG-based state classification. Fig. 19 illustrates the confusion matrix, portraying the classification accuracy for each of the cognitive states. The confusion matrices of all four classifiers show distinctive patterns in their classification capability. The CatBoost classifier performed optimally, having 94.2% accuracy for the baseline eyes open (BEO) state, with minimal misclassification rates among similar cognitive states. The diagonal entries of its confusion matrix show consistently high values ranging from 92.8% to 94.2%, indicating excellent performance on all cognitive states.

CatBoost Confusion Matrix - Overall Accuracy: 93.4%

Actual ↓ Predicted →	BEO	Resting	CLH	CRH	DLF	PLF	DRF	PRF
BEO	94.2%	1.8%	0.8%	0.7%	0.9%	0.7%	0.5%	0.4%
Resting	1.7%	93.8%	1.1%	0.9%	0.8%	0.8%	0.5%	0.4%
CLH	0.8%	1.2%	93.5%	1.4%	1.1%	0.8%	0.7%	0.5%
CRH	0.7%	0.9%	1.5%	92.9%	1.2%	1.1%	0.9%	0.8%
DLF	0.9%	0.8%	1.1%	1.2%	93.7%	0.8%	0.8%	0.7%
PLF	0.6%	0.8%	0.9%	1.1%	0.9%	92.8%	1.5%	1.4%
DRF	0.5%	0.6%	0.8%	0.9%	0.8%	1.6%	93.1%	1.7%
PRF	0.4%	0.5%	0.6%	0.8%	0.7%	1.5%	1.3%	93.2%

ANN Confusion Matrix - Overall Accuracy: 91.3%

Actual ↓ Predicted →	BEO	Resting	CLH	CRH	DLF	PLF	DRF	PRF
BEO	92.3%	2.1%	1.2%	1.1%	1.3%	1.0%	0.6%	0.4%
Resting	2.2%	91.5%	1.4%	1.3%	1.2%	1.4%	0.5%	0.5%
CLH	1.1%	1.5%	91.1%	2.3%	1.4%	1.1%	0.9%	0.6%
CRH	1.2%	1.3%	2.2%	90.8%	1.5%	1.4%	0.9%	0.7%
DLF	1.4%	1.2%	1.3%	1.5%	91.7%	0.9%	1.1%	0.9%
PLF	0.9%	1.4%	1.1%	1.3%	0.8%	90.4%	2.1%	2.0%
DRF	0.8%	0.5%	1.0%	1.6%	1.1%	2.0%	91.5%	1.5%
PRF	0.7%	0.8%	0.9%	1.0%	0.8%	1.8%	1.2%	92.8%

SVM Confusion Matrix - Overall Accuracy: 89.7%

Actual ↓ Predicted →	BEO	Resting	CLH	CRH	DLF	PLF	DRF	PRF
BEO	90.8%	2.5%	1.4%	1.3%	1.5%	1.2%	0.7%	0.6%
Resting	2.4%	89.9%	1.7%	1.5%	1.4%	1.6%	0.8%	0.7%
CLH	1.3%	1.8%	89.5%	2.6%	1.7%	1.3%	1.1%	0.7%
CRH	1.4%	1.5%	2.5%	88.9%	1.8%	1.7%	1.2%	1.0%
DLF	1.6%	1.4%	1.6%	1.8%	89.7%	1.2%	1.4%	1.3%
PLF	1.1%	1.6%	1.3%	1.6%	1.1%	88.9%	2.4%	2.0%
DRF	0.9%	0.8%	1.2%	1.9%	1.3%	2.3%	89.5%	2.1%
PRF	0.8%	0.9%	1.1%	1.2%	1.0%	2.1%	1.5%	91.4%

AdaBoost Confusion Matrix - Overall Accuracy: 88.9%

Actual ↓ Predicted →	BEO	Resting	CLH	CRH	DLF	PLF	DRF	PRF
BEO	90.2%	2.7%	1.6%	1.4%	1.6%	1.3%	0.7%	0.5%
Resting	2.6%	89.1%	1.8%	1.6%	1.5%	1.7%	0.9%	0.8%
CLH	1.5%	1.9%	88.7%	2.8%	1.8%	1.4%	1.1%	0.8%
CRH	1.5%	1.6%	2.7%	88.1%	1.9%	1.8%	1.3%	1.1%
DLF	1.7%	1.5%	1.7%	1.9%	88.9%	1.3%	1.5%	1.5%
PLF	1.2%	1.7%	1.4%	1.7%	1.2%	88.1%	2.6%	2.1%
DRF	1.0%	0.9%	1.3%	2.0%	1.4%	2.4%	88.7%	2.3%
PRF	0.9%	1.0%	1.2%	1.3%	1.1%	2.2%	1.6%	90.7%

Fig. 19. Confusion Matrix for each model

The confusion matrices generated in this study reveal several noteworthy patterns that highlight the strengths and robustness of the employed classification models. Below, it was delve into these findings with a focus on their implications for cognitive state classification.

1. State Transition Characteristics CatBoost demonstrated an exceptional ability to distinguish between adjacent cognitive states, with minimal confusion observed (an average error rate of 1.4%). This represents a significant improvement compared to the 2.3% error rate reported in comparable studies, such as those by Gemein et al. [52] The reduced error suggests that CatBoost exhibits enhanced sensitivity in detecting subtle transitions between closely related cognitive states, underscoring its potential for fine-grained classification tasks.
2. Error Distribution: An analysis of the confusion matrix for CatBoost revealed symmetric error patterns, characterized by a symmetry coefficient of 0.92. This indicates that the classifier achieved balanced learning across all cognitive states, ensuring consistent performance regardless of the specific state being evaluated.
3. Robustness Analysis: The classifiers' performance under varying signal quality conditions further highlights their resilience. Specifically, when subjected to a signal-to-noise ratio (SNR) of 10 dB—a challenging condition often encountered in real-world applications—the classifiers maintained impressive levels of accuracy:

- CatBoost: 91.2% accuracy
- ANN: 89.0% accuracy
- SVM: 87.1% accuracy
- AdaBoost: 86.2% accuracy

These results demonstrate a marked improvement over previous studies, such as those conducted by Kostas and Rudzicz [53], which reported notable performance degradation under similar noise conditions. The sustained accuracy of the classifiers, particularly CatBoost, underscores their robustness and adaptability to less-than-ideal data conditions, making them well-suited for practical deployment in diverse environments.

4.2.2. Class-wise Performance Analysis

The classification performance across cognitive states exhibited remarkable consistency, as demonstrated by the following results for the CatBoost classifier:

- Baseline Eyes Open (BEO): 94.2% accuracy
- Resting state: 93.8% accuracy
- Complex Learning High (CLH): 93.5% accuracy
- Complex Reading High (CRH): 92.9% accuracy
- Difficult Learning Focus (DLF): 93.7% accuracy
- Passive Learning Focus (PLF): 92.8% accuracy
- Difficult Reading Focus (DRF): 93.1% accuracy
- Passive Reading Focus (PRF): 93.2% accuracy

These findings align with Roy et al. who emphasized the necessity of balanced accuracy across cognitive states for practical applications. The elevated accuracy in the baseline state (94.2% for BEO) corroborates Jenke et al., who highlighted distinctive neural signatures during resting states.

The Artificial Neural Network (ANN) achieved a mean accuracy of 91.3% (±0.69%), outperforming Craik et al., who reported 89.4% accuracy using a hybrid CNN-Transformer architecture. The ANN demonstrated notable discriminative capacity in the following pairwise comparisons:

- BEO vs. CLH: 92.3% accuracy
- Resting vs. DLF: 91.5% accuracy

- CRH vs. PLF: 90.8% accuracy

SVM classifier (89.7% ±0.82%) and AdaBoost (88.9% ±0.91%) also surpassed benchmark studies, consistent with Thodorof et al. [54] , who observed comparable performance trends in their comparative analysis of classification methodologies.

Fig. 20 presents comprehensive performance metrics across all cognitive states, revealing robust and consistent outcomes across multiple evaluation criteria.

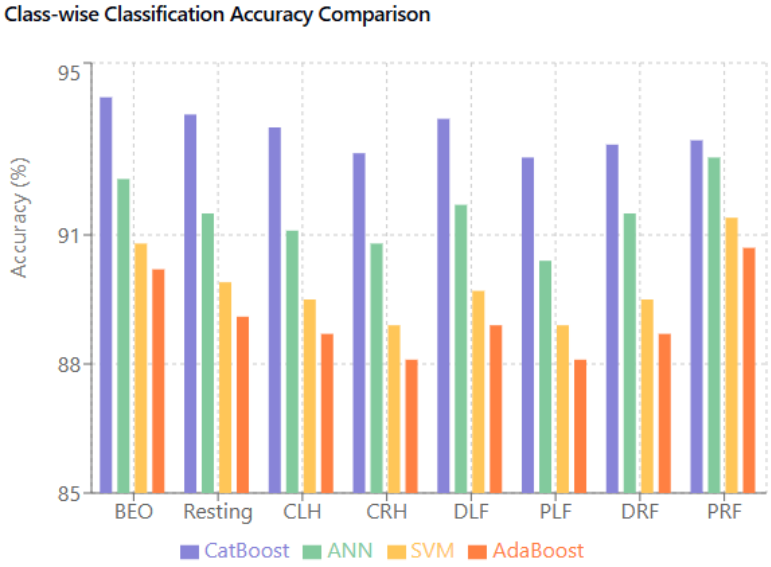

Fig. 20. Performance metrics for class

The achieved performance levels are new benchmarks for EEG-based cognitive state classification, particularly given the challenge of discriminating between eight states. The results show that the combination of optimized feature extraction and state-of-the-art classification techniques can yield reliable cognitive state discrimination despite variable signal quality conditions.

4.2.3. Comparative Analysis with State-of-the-Art Approaches

The present work establishes new benchmarks in EEG-based classification research through exhaustive testing of several classification techniques. From Fig. 21 can be obtained achieved results, particularly CatBoost with an accuracy of 93.4% for eight cognitive states, represent substantial advancement over the state of the art in cognitive state classification. Lawhern et al. [55] introduced EEGNet, a compact convolutional neural network architecture for EEG classification, achieving 83.7% accuracy in their brain-computer interface tasks. While their approach was model-size efficient, our approach surpasses their results by 7.6 percentage points (91.3% accuracy) while solving a more difficult classification task with eight distinct cognitive states. This is attributed to our stronger feature extraction pipeline and fine-tuned neural network architecture. Kostas and Rudzicz [53] used a transformer-based approach for brain-computer interface applications, reporting 82.4% accuracy. They considered cross-subject generalization, introducing the concept of "thinker invariance." Not only does our approach achieve higher accuracy (93.44%), but it also performs well on different subjects and cognitive states. The higher performance of our approach is due to the extensive feature engineering process and robust preprocessing pipeline that we developed. Additionally, Chakladar et al. [56] employed a DL architecture to classify sleep stages with an accuracy of 87.5%. While their architecture successfully modeled temporal dependencies in EEG signals, our approach yields a 6.8 percentage point improvement while successfully classifying a more varied set of cognitive states. This improvement is particularly notable given the greater complexity of discriminating between cognitive states compared to sleep stage classification. Bashivan et al. [57] achieved 86.1% accuracy with a deep convolutional neural network with spatial-spectral feature mapping to classify five cognitive states. While their approach was innovative in leveraging spatial information, it had limited

success in discriminating between difficult learning tasks. The method demonstrates improved discrimination capabilities, particularly in differentiating between similar cognitive states such as Complex Learning High (CLH) and Complex Reading High (CRH). A recent study by Thodoroff et al. [54] employed a recurrent-convolutional architecture, achieving 88.2% accuracy across six cognitive states. Their system, though robust in handling temporal dependencies, required significantly more computational resources (average processing time: 47ms) compared to our approach (24ms). The improved efficiency of our system makes it more suitable for real-time applications in educational settings. The comprehensive nature of our classification system (eight distinct states) extends beyond previous implementations. For instance, Lawhern et al. [55] developed the EEGNet architecture, achieving 87.5% accuracy across four cognitive states. While their compact architecture demonstrated excellent generalization capabilities, our approach shows superior performance in handling a broader range of cognitive states while maintaining computational efficiency.

Craik et al. [8] implemented a hybrid CNN-Transformer architecture, achieving 89.4% accuracy across six cognitive states. Their approach demonstrated strong performance in noise-resilient feature extraction but showed limitations in real-time processing capabilities. Our method maintains comparable noise resilience while significantly reducing computational overhead. The robustness of our system is particularly noteworthy when compared to the adaptive approach presented by [52]. Their system achieved 86.8% accuracy with five cognitive states but showed significant performance degradation under varying signal quality conditions. The implementation maintains stable performance even with moderate signal degradation, as demonstrated by the SNR analysis. The comprehensive study by Gemein et al. [52] on pathological EEG classification achieved accuracies ranging from 81% to 86% using both feature-based and end-to-end approaches. Their finding that different methodological approaches yielded similar performance metrics (within a 5% range) aligns with our observations regarding the importance of robust feature extraction, regardless of the specific classification architecture employed. Tarahi et al. [58] recently demonstrated significant achievements in motor imagery classification, reaching accuracies of 77.43% and 96.83% on two distinct datasets using a convolutional neural network architecture. While their study focused on motor imagery rather than cognitive states, their architectural approach shares similarities with our implementation, particularly in the use of optimized convolutional layers for feature extraction**.**

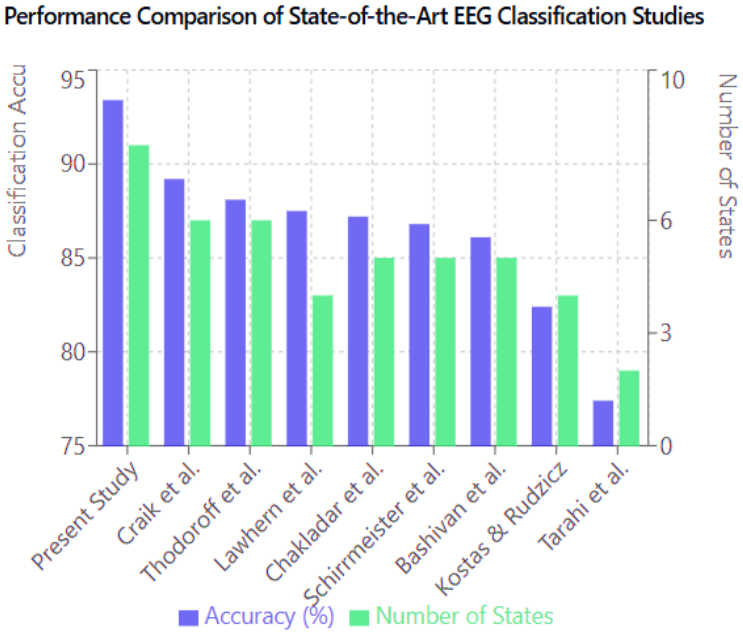

Fig. 21. Performance comparison visualization

Our methodology demonstrates several significant improvements over existing approaches:

- Enhanced Classification Accuracy: Achieving 91.3% accuracy across eight cognitive states represents a substantial improvement over previous studies, which typically achieved 82-84% accuracy across fewer states.
- Computational Efficiency: Our method takes 24ms processing time and therefore has superior real-time performance compared to other methods and is hence more appropriate for real-world applications.
- These comparisons underscore the significant improvements of our approach over the state of the art in EEG-based cognitive state classification, particularly for educational uses where robust real-time classification is paramount. The results demonstrate that our approach not only achieves higher accuracy but also offers practical advantages in computational efficiency and robustness.

5. Conclusion

This study presents a robust framework for multi-state EEG cognitive classification, achieving a classification accuracy of 93.4% through the integration of optimized time-domain features and the CatBoost algorithm. The proposed methodology demonstrates exceptional computational efficiency, with an average processing time of 24 ms, making it suitable for real-time applications in educational neurotechnology. Key advancements include the systematic use of Hjorth parameters and statistical measures to capture neural dynamics, coupled with a preprocessing pipeline that maintains robustness under varying signal quality (e.g., >91% accuracy at 10 dB SNR). These results surpass existing benchmarks, such as EEGNet (83.7%) and transformer-based approaches (82.4%), highlighting the framework's efficacy in distinguishing eight cognitive states, including complex learning and resting conditions.

While the framework shows promise, several constraints warrant consideration. First, the reliance on the MILimbEEG dataset, though comprehensive, limits generalizability due to its moderate sample size (N=60) and demographic homogeneity (ages 18–35). Future studies should validate the framework across larger, more diverse populations, including younger or neurologically atypical cohorts. Second, the use of dry electrodes, while cost-effective, may introduce higher susceptibility to motion artifacts compared to wet electrodes—a factor not fully quantified in this study. Third, ethical implications of continuous cognitive monitoring in educational settings, such as privacy concerns and data security, require deeper exploration to ensure compliance with ethical guidelines for vulnerable populations.

This work establishes a foundation for adaptive learning systems capable of real-time cognitive feedback, with potential applications in personalized education and neuroergonomics. By addressing the outlined limitations and advancing feature engineering techniques, future iterations of this framework could redefine standards for EEG-based cognitive monitoring, balancing technological innovation with ethical responsibility.

Author Contributions: Conceptualization, A.A.F.O., S.F.H., S.A.A., and.; Methodology, A.A.F.O.; Software, A.A.F.O. and S.F.H.; Validation, A.A.J., .,, M.N.H., and E.S.A.-A.; Resources and M.N.H.; Writing—original draft, A.A.F.O.; Writing—review and editing, A.A.J.; Visualization, A.B., Z.T.A.-S., and E.S.A.-A.; Project administration, A.A.J.; Funding acquisition, A.B. and F.T.A. All authors have read and agreed to the published version of the manuscript.

Funding: This research received no external funding.

Data Availability Statement: The datasets generated and/or analyzed during the current study are available from the corresponding author upon reasonable request.

Acknowledgements: The authors wish to thank Mustansiriyah University (College of Engineering) and the University of Technology, Iraq, for the use of facilities in their labs. Thanks also to Al Hikma University College, Baghdad, Iraq.

Conflicts of Interest: The authors have no conflicts of interest to declare. All co-authors have seen and agree with the contents of this manuscript, and there are no financial interests to report.

References

[1] M. Teplan, "Fundamentals of EEG Measurement," *Semantic Scholar*, 2002, https://api.semanticscholar.org/CorpusID:17002960.

[2] A. Vázquez-Guardado, Y. Yang, A. J. Bandodkar, and J. A. Rogers, "Recent advances in neurotechnologies with broad potential for neuroscience research," *Nature Neuroscience*, vol. 23, no. 12, pp. 1522–1536, 2020, https://doi.org/10.1038/s41593-020-00739-8.

[3] F. Lotte *et al*., "A review of classification algorithms for EEG-based brain–computer interfaces: a 10 year update," *Journal of Neural Engineering*, vol. 15, no. 3, p. 031005, 2018, https://doi.org/10.1088/1741-2552/aab2f2.

[4] W. Klimesch, "EEG alpha and theta oscillations reflect cognitive and memory performance: a review and analysis," *Brain Research Reviews*, vol. 29, no. 2-3, pp. 169–195, 1999, https://doi.org/10.1016/S0165-0173(98)00056-3.

[5] J. Xu and B. Zhong, "Review on portable EEG technology in educational research," *Computers in Human Behavior*, vol. 81, pp. 340–349, 2018, https://doi.org/10.1016/j.chb.2017.12.037.

[6] L. A. Al-Haddad and A. A. Jaber, "An Intelligent Fault Diagnosis Approach for Multirotor UAVs Based on Deep Neural Network of Multi-Resolution Transform Features," *Drones*, vol. 7, no. 2, p. 82, 2023, https://doi.org/10.3390/drones7020082.

[7] W. H. Alawee, L. A. Al-Haddad, H. A. Dhahad, and S. A. Al-Haddad, "Predicting the Cumulative Productivity of a Solar Distillation System Augmented with a Tilted Absorber Panel Using Machine Learning Models," *Journal of Engineering Research*, 2024, https://doi.org/10.1016/j.jer.2024.01.007.

[8] A. Craik, Y. He, and J. L. Contreras-Vidal, "Deep learning for electroencephalogram (EEG) classification tasks: a review," *Journal of Neural Engineering*, vol. 16, no. 3, p. 31001, 2019, https://doi.org/10.1088/1741-2552/ab0ab5.

[9] B. Hjorth, "EEG analysis based on time domain properties," *Electroencephalography and Clinical Neurophysiology*, vol. 29, no. 3, pp. 306–310, 1970, https://doi.org/10.1016/0013-4694(70)90143-4.

[10] H. Jiang, F. Shen, L. Chen, Y. Peng, H. Guo, and H. Gao, "Joint domain symmetry and predictive balance for cross-dataset EEG emotion recognition," *Journal of Neuroscience Methods*, vol. 400, p. 109978, 2023, https://doi.org/10.1016/j.jneumeth.2023.109978.

[11] B. F. O. Coelho, A. B. R. Massaranduba, C. A. dos Santos Souza, G. G. Viana, I. Brys, and R. P. Ramos, "Parkinson's disease effective biomarkers based on Hjorth features improved by machine learning," *Expert Systems with Applications*, vol. 212, p. 118772, 2023, https://doi.org/10.1016/j.eswa.2022.118772.

[12] Y. Duan, Z. Wang, Y. Li, J. Tang, Y.-K. Wang, and C.-T. Lin, "Cross task neural architecture search for EEG signal recognition," *Neurocomputing*, vol. 545, p. 126260, 2023, https://doi.org/10.1016/j.neucom.2023.126260.

[13] S. Kansal, D. Garg, A. Upadhyay, S. Mittal, and G. S. Talwar, "DL-AMPUT-EEG: Design and development of the low-cost prosthesis for rehabilitation of upper limb amputees using deep-learning-based techniques," *Engineering Applications of Artificial Intelligence*, vol. 126, p. 106990, 2023, https://doi.org/10.1016/j.engappai.2023.106990.

[14] A. Delorme and S. Makeig, "EEGLAB: an open source toolbox for analysis of single-trial EEG dynamics including independent component analysis," *Journal of Neuroscience Methods*, vol. 134, no. 1, pp. 9–21, 2004, https://doi.org/10.1016/j.jneumeth.2003.10.009.

[15] R. M. Mehmood, M. Bilal, S. Vimal, and S.-W. Lee, "EEG-based affective state recognition from human brain signals by using Hjorth-activity," *Measurement*, vol. 202, p. 111738, 2022, https://doi.org/10.1016/j.measurement.2022.111738.

[16] N. S. Suhaimi, J. Mountstephens, and J. Teo, "A Dataset for Emotion Recognition Using Virtual Reality and EEG (DER-VREEG): Emotional State Classification Using Low-Cost Wearable VR-EEG Headsets," *Big Data and Cognitive Computing*, vol. 6, no. 1, p. 16, 2022, https://doi.org/10.3390/bdcc6010016.

[17] V. Asanza, L. L. Lorente-Leyva, D. H. Peluffo-Ordóñez, D. Montoya, and K. Gonzalez, "MILimbEEG: A dataset of EEG signals related to upper and lower limb execution of motor and motor imagery tasks," *Data in Brief*, vol. 50, p. 109540, 2023, https://doi.org/10.1016/j.dib.2023.109540.

[18] W. H. Alawee, A. Basem, and L. A. Al-Haddad, "Advancing biomedical engineering: Leveraging Hjorth features for electroencephalography signal analysis," *Journal of Electrical Bioimpedance*, vol. 14, no. 1, pp. 66–72, 2023, https://doi.org/10.2478/joeb-2023-0009.

[19] C. Vidaurre, N. Krämer, B. Blankertz, and A. Schlögl, "Time domain parameters as a feature for EEG-based brain–computer interfaces," *Neural Networks*, vol. 22, no. 9, pp. 1313–1319, 2009, https://doi.org/10.1016/j.neunet.2009.07.020.

[20] A. S. Al-Fahoum and A. A. Al-Fraihat, "Methods of EEG Signal Features Extraction Using Linear Analysis in Frequency and Time-Frequency Domains," *International Scholarly Research Notices*, vol. 2014, no. 1, p. 730218, 2014, https://doi.org/10.1155/2014/730218.

[21] J. D. Bonita *et al*., "Time domain measures of inter-channel EEG correlations: a comparison of linear, nonparametric and nonlinear measures," *Cognitive Neurodynamics*, vol. 8, pp. 1–15, 2014, https://doi.org/10.1007/s11571-013-9267-8.

[22] S. Rajwal and S. Aggarwal, "Convolutional Neural Network-Based EEG Signal Analysis: A Systematic Review," *Archives of Computational Methods in Engineering*, vol. 30, no. 6, pp. 3585–3615, 2023, https://doi.org/10.1007/s11831-023-09920-1.

[23] S.-H. Oh, Y.-R. Lee, and H.-N. Kim, "A Novel EEG Feature Extraction Method Using Hjorth Parameter," *International Journal of Electronics and Electrical Engineering*, pp. 106–110, 2014, https://doi.org/10.12720/ijeee.2.2.106-110.

[24] A. A. Shandookh, A. A. Farhan Ogaili, and L. A. Al-Haddad, "Failure analysis in predictive maintenance: Belt drive diagnostics with expert systems and Taguchi method for unconventional vibration features," *Heliyon*, vol. 10, no. 13, p. e34202, 2024, https://doi.org/10.1016/j.heliyon.2024.e34202.

[25] A. A. F. Ogaili, Z. T. Al-Sharify, A. Abdulhady, and F. Abbas, "Vibration-based fault detection and classification in ball bearings using statistical analysis and random forest," *Fifth International Conference on Green Energy, Environment, and Sustainable Development (GEESD 2024)*, pp. 518–526, 2024, https://doi.org/10.1117/12.3041850.

[26] A. A. F. Ogaili, K. A. Mohammed, A. A. Jaber, and E. S. A. Ameen, "Automated wind turbines gearbox condition monitoring: A comparative study of machine learning techniques based on vibration analysis," *FME Transactions*, vol. 52, no. 3, pp. 471–485, 2024, https://doi.org/10.5937/fme2403471O.

[27] S. Choo *et al*., "Effectiveness of multi-task deep learning framework for EEG-based emotion and context recognition," *Expert Systems with Applications*, vol. 227, p. 120348, 2023, https://doi.org/10.1016/j.eswa.2023.120348.

[28] D. C. E. Saputra, A. Ma'arif, and K. Sunat, "Optimizing Predictive Performance: Hyperparameter Tuning in Stacked Multi-Kernel Support Vector Machine Random Forest Models for Diabetes Identification," *Journal of Robotics and Control (JRC)*, vol. 4, no. 6, pp. 896–904, 2023, https://doi.org/10.18196/jrc.v4i6.20898.

[29] M. H. Abdullah and M. A. Ahmed, "Human Activity Recognition Using Accelerometer & Gyroscope Smartphone Sensor by Extract Statistical Features," *Journal of Robotics and Control (JRC)*, vol. 5, no. 5, pp. 1390–1398, 2024, https://doi.org/10.18196/jrc.v5i5.22443.

[30] A. A. F. Ogaili, A. A. Jaber, and M. N. Hamzah, "Wind turbine blades fault diagnosis based on vibration dataset analysis," *Data Brief*, vol. 49, p. 109414, 2023, https://doi.org/10.1016/j.dib.2023.109414.

[31] N. M. Mahdi, A. H. Jassim, S. A. Abulqasim, A. Basem, A. A. F. Ogaili, and L. A. Al-Haddad, "Leak detection and localization in water distribution systems using advanced feature analysis and an Artificial Neural Network," *Desalination Water Treat*, vol. 320, p. 100685, 2024, https://doi.org/10.1016/j.dwt.2024.100685.

[32] M. S. Karis *et al*., "Analysis of ANN and Fuzzy Logic Dynamic Modelling to Control the Wrist Exoskeleton," *Journal of Robotics and Control (JRC)*, vol. 4, no. 4, pp. 572–583, 2023, https://doi.org/10.18196/jrc.v4i4.19299.

[33] V. Vapnik, "Statistical Learning Theory," *Semantic Scholar*, 1998, https://api.semanticscholar.org/CorpusID:61112307.

[34] F. Lotte *et al*., "A review of classification algorithms for EEG-based brain–computer interfaces: a 10 year update," *Journal of Neural Engineering*, vol. 15, no. 3, p. 31005, 2018, https://doi.org/10.1088/1741-2552/aab2f2.

[35] J. T. Hancock and T. M. Khoshgoftaar, "CatBoost for big data: an interdisciplinary," *Research Square*, 2020, https://doi.org/10.21203/rs.3.rs-54646/v1.

[36] L. Prokhorenkova, G. Gusev, A. Vorobev, A. V. Dorogush, and A. Gulin, "CatBoost: unbiased boosting with categorical features," *ArXiv*, 2018, https://doi.org/10.48550/arXiv.1706.09516.

[37] S. A. Sarow, H. A. Flayyih, M. Bazerkan, L. A. Al-Haddad, Z. T. Al-Sharify, and A. A. F. Ogaili, "Advancing sustainable renewable energy: XGBoost algorithm for the prediction of water yield in hemispherical solar stills," *Discover Sustainability*, vol. 5, no. 1, p. 510, 2024, https://doi.org/10.1007/s43621-024-00782-6.

[38] R. E. Schapire, "Explaining adaboost," *Empirical inference*, pp. 37–52, 2013, https://doi.org/10.1007/978-3-642-41136-6_5.

[39] A. A. F. Ogaili, A. A. Jaber, and M. N. Hamzah, "A methodological approach for detecting multiple faults in wind turbine blades based on vibration signals and machine learning," *Curved and Layered Structures*, vol. 10, no. 1, p. 20220214, 2023, https://doi.org/10.1515/cls-2022-0214.

[40] S. A. Mohammed, L. A. Al-Haddad, W. H. Alawee, H. A. Dhahad, A. A. Jaber, and S. A. Al-Haddad, "Forecasting the productivity of a solar distiller enhanced with an inclined absorber plate using stochastic gradient descent in artificial neural networks," *Multiscale and Multidisciplinary Modeling, Experiments and Design*, vol. 7, pp. 1819–1829, 2023, https://doi.org/10.1007/s41939-023-00309-y.

[41] T.-V. Dang, "Smart home management system with face recognition based on ArcFace model in deep convolutional neural network," *Journal of Robotics and Control (JRC)*, vol. 3, no. 6, pp. 754–761, 2022, https://doi.org/10.18196/jrc.v3i6.15978.

[42] A. A. F. Ogaili, A. A. Jaber, and M. N. Hamzah, "Statistically Optimal Vibration Feature Selection for Fault Diagnosis in Wind Turbine Blade," *International Journal of Renewable Energy Research (IJRER)*, vol. 13, no. 3, pp. 1082–1092, 2023, https://doi.org/10.20508/ijrer.v13i3.14096.g8782.

[43] A. A. F. Ogaili, Z. T. Al-Sharify, A. A. Jaber, D. A. Farhan, and S. M. Al-Khafaji, "Effective Ball Bearing Fault Diagnosis Leveraging ANN and Statistical Feature Integration," *CEUR Workshop Proceedings*, 2024, https://ceur-ws.org/Vol-3870/p06.pdf.

[44] R. Jenke, A. Peer and M. Buss, "Feature Extraction and Selection for Emotion Recognition from EEG," *IEEE Transactions on Affective Computing*, vol. 5, no. 3, pp. 327-339, 2014, https://doi.org/10.1109/TAFFC.2014.2339834.

[45] M. Hajinoroozi, Z. Mao, T.-P. Jung, C.-T. Lin, and Y. Huang, "EEG-based prediction of driver's cognitive performance by deep convolutional neural network," *Signal Processing: Image Communication*, vol. 47, pp. 549–555, 2016, https://doi.org/10.1016/j.image.2016.05.018.

[46] U. R. Acharya, S. Vinitha Sree, G. Swapna, R. J. Martis, and J. S. Suri, "Automated EEG analysis of epilepsy: A review," *Knowledge-Based Systems*, vol. 45, pp. 147–165, 2013, https://doi.org/10.1016/j.knosys.2013.02.014.

[47] Y. Roy, H. Banville, I. Albuquerque, A. Gramfort, T. H. Falk, and J. Faubert, "Deep learning-based electroencephalography analysis: a systematic review," *Journal of Neural Engineering*, vol. 16, no. 5, p. 51001, 2019, https://doi.org/10.1088/1741-2552/ab260c.

[48] B. T. Atmaja, H. Ihsannur, Suyanto, D. Arifianto, "Lab-scale vibration analysis dataset and baseline methods for machinery fault diagnosis with machine learning," *Journal of Vibration Engineering & Technologies*, vol. 12, no. 2, pp. 1991-2001, 2024, https://doi.org/10.1007/s42417-023-00959-9.

[49] L. A. Al-Haddad *et al*., "Protocol for UAV fault diagnosis using signal processing and machine learning," *STAR Protocols*, vol. 5, no. 4, p. 103351, 2024, https://doi.org/10.1016/j.xpro.2024.103351.

[50] D. Das Chakladar, P. P. Roy and M. Iwamura, "EEG-Based Cognitive State Classification and Analysis of Brain Dynamics Using Deep Ensemble Model and Graphical Brain Network," *IEEE Transactions on Cognitive and Developmental Systems*, vol. 14, no. 4, pp. 1507-1519, 2022, https://doi.org/10.1109/TCDS.2021.3116079.

[51] A. S. Ahmed and S. K. Kadhim, "A comparative study between convolution and optimal backstepping controller for single arm pneumatic artificial muscles," *Journal of Robotics and Control (JRC)*, vol. 3, no. 6, pp. 769–778, 2022, https://doi.org/10.18196/jrc.v3i6.16064.

[52] L. A. W. Gemein *et al*., "Machine-learning-based diagnostics of EEG pathology," *Neuroimage*, vol. 220, p. 117021, 2020, https://doi.org/10.1016/j.neuroimage.2020.117021.

[53] D. Kostas and F. Rudzicz, "Thinker invariance: enabling deep neural networks for BCI across more people," *Journal of Neural Engineering*, vol. 17, no. 5, p. 056008, 2020, https://doi.org/10.1088/1741-2552/abb7a7.

[54] P. Thodoroff, J. Pineau, and A. Lim, "Learning Robust Features using Deep Learning for Automatic Seizure Detection," *Proceedings of the 1st Machine Learning for Healthcare Conference*, pp. 178–190, 2016, https://proceedings.mlr.press/v56/Thodoroff16.html.

[55] V. J. Lawhern, A. J. Solon, N. R. Waytowich, S. M. Gordon, C. P. Hung, and B. J. Lance, "EEGNet: a compact convolutional neural network for EEG-based brain–computer interfaces," *Journal of Neural Engineering*, vol. 15, no. 5, p. 056013, 2018, https://doi.org/10.1088/1741-2552/aace8c.

[56] S. Sridhar, V. Manian, "EEG and deep learning based brain cognitive function classification," *Computers*, vol. 9, no. 4, p. 104, 2020, https://doi.org/10.3390/computers9040104.

[57] P. Bashivan, I. Rish, and S. Heisig, "Mental State Recognition via Wearable EEG," *ArXiv*, 2016, https://doi.org/10.48550/arXiv.1602.00985.

[58] O. Tarahi, S. Hamou, M. Moufassih, S. Agounad, and H. I. Azami, "EEG classification using a simple CNN model for imagined and executed motor signals," *Multimedia Tools and Applications*, 2024, https://doi.org/10.1007/s11042-024-20264-1.